Nanoclustering phase competition induces the resistivity hump in colossal magnetoresistive manganites

Kalpataru Pradhan[1,2,*] and Seiji Yunoki[2,3,4,†]

[1]*CMP Division, Saha Institute of Nuclear Physics, HBNI, Kolkata 700064, India*

[2]*Computational Quantum Matter Research Team, RIKEN, Center for Emergent Matter Science (CEMS), Saitama 351-0198, Japan*

[3]*Computational Condensed Matter Physics Laboratory, RIKEN, Wako, Saitama 351-0198, Japan*

[4]*Computational Materials Science Research Team, RIKEN Advanced Institute for Computational Science (AICS), Hyogo 650-0047, Japan*

(Received 26 September 2017; published 11 December 2017)

Using a two-band double-exchange model with Jahn-Teller lattice distortions and superexchange interactions, supplemented by quenched disorder, at an electron density $n = 0.65$, we explicitly demonstrate the coexistence of the $n = 1/2$-type (π,π) charge-ordered and the ferromagnetic nanoclusters above the ferromagnetic transition temperature T_c in colossal magnetoresistive (CMR) manganites. The resistivity increases due to the enhancement of the volume fraction of the charge-ordered and the ferromagnetic nanoclusters upon decreasing the temperature down to T_c. The ferromagnetic nanoclusters start to grow and merge, and the volume fraction of the charge-ordered nanoclusters decreases below T_c, leading to the sharp drop in the resistivity. By applying a small external magnetic field h, we show that the resistivity above T_c increases, as compared with the case when $h = 0$, a fact that further confirms the coexistence of the charge-ordered and the ferromagnetic nanoclusters. In addition, we show that the volume fraction of the charge-ordered nanoclusters decreases upon increasing the bandwidth, and consequently the resistivity hump diminishes for large bandwidth manganites, in good qualitative agreement with experiments. The obtained insights from our calculations provide a complete pathway to understand the phase competition in CMR manganites.

DOI: 10.1103/PhysRevB.96.214416

I. INTRODUCTION

The strong coupling between charge, spin, orbital, and lattice degrees of freedom, supplemented by weak disorder, leads to unusual colossal response phenomena in manganites [1–4]. There has been intense focus over the past two decades to validate the phase coexistence/competition scenario [5–18], which is believed to be a necessary ingredient to explain the resistivity hump in colossal magnetoresistive (CMR) manganites. Furthermore, understanding the phase competition in bulk manganites helps in designing low-dimensional manganite nanostructures with emergent physical phenomena [19–21].

The manganites, materials of the form $R_{1-x}A_xMnO_3$, where R denotes rare-earth elements (La, Nd, Pr, etc.) and A denotes alkaline-earth elements (Ca, Sr, and Ba), are best known for their CMR property in the doping range $x = 1 - n = 0.3$–0.4 (n is the electron density). The bandwidth of the manganites increases with the mean radius r_A of R and A ions [22,23], and the size mismatch between the two radii controls the strength of the cation disorder [24,25]. Figure 1(a), reproduced from Ref. [23], schematically summarizes a phase diagram of the manganites. Low-temperature magnetic states for $n = 0.5$ and 0.65 are also listed in Table I along with ionic radii of different R and A ions.

The phase competition arising due to the proximity of a variety of phases, in the presence of cationic disorder, often leads to novel phenomena such as inhomogeneities, phase coexistence, and percolative transport [3,4]. Recent experiments [15–18] show that nanoscale ferromagnetic (FM) regions and $n = 1/2$-type (π,π) charge-ordered (CO) [5] regions, which characterizes the CE-type phase, coexist above the FM transition temperature T_c. The precise microscopic origin of the phase competition above T_c is still elusive theoretically [26,27]. The absence of FM correlations above T_c fails to establish the phase competition scenario in CMR manganites in recent theoretical studies [28,29].

In this paper, we explicitly demonstrate the phase competition between the $n = 1/2$-type (π,π) CO nanoclusters and the FM nanoclusters at $n = 0.65$, relevant to the CMR manganites, above the FM T_c. Our study reveals that this phase competition induces the resistivity hump, and is expected only in those manganites for which the ground state is the CE-type phase at $n \sim 0.5$. Upon increasing the bandwidth, the volume fraction of the CO nanoclusters decreases and consequently the resistivity hump around T_c vanishes.

II. MODEL HAMILTONIAN AND METHOD

We consider the following two-band model Hamiltonian [3], a minimal model that is required to capture the essential phases in manganites [30–33], in two spatial dimensions:

$$H = -\sum_{\langle ij\rangle,s}\sum_{\alpha,\beta} t^{ij}_{\alpha\beta} c^\dagger_{i\alpha s} c_{j\beta s} - J_H \sum_i \mathbf{S}_i \cdot \boldsymbol{\sigma}_i + J \sum_{\langle ij\rangle} \mathbf{S}_i \cdot \mathbf{S}_j - \lambda \sum_i \mathbf{Q}_i \cdot \boldsymbol{\tau}_i + \frac{K}{2}\sum_i \mathbf{Q}_i^2 + \sum_i (\epsilon_i - \mu) n_i, \quad (1)$$

where $c^\dagger_{i\alpha s}$ is the electron creation operator at site i with orbital $\alpha = (a,b)$ and spin $s (= \uparrow,\downarrow)$. The kinetic energy term includes inter- and intraorbital nearest-neighbor hopping $t^{ij}_{\alpha\beta}$, i.e., $t^x_{aa} = t^y_{aa} \equiv t$, $t^x_{bb} = t^y_{bb} \equiv t/3$, $t^x_{ab} = t^x_{ba} \equiv -t/\sqrt{3}$, and $t^y_{ab} = t^y_{ba} \equiv t/\sqrt{3}$ along x and y directions, where a and b refer to two Mn e_g orbitals $d_{x^2-y^2}$ and $d_{3z^2-r^2}$, respectively.

*kalpataru.pradhan@saha.ac.in

†yunoki@riken.jp

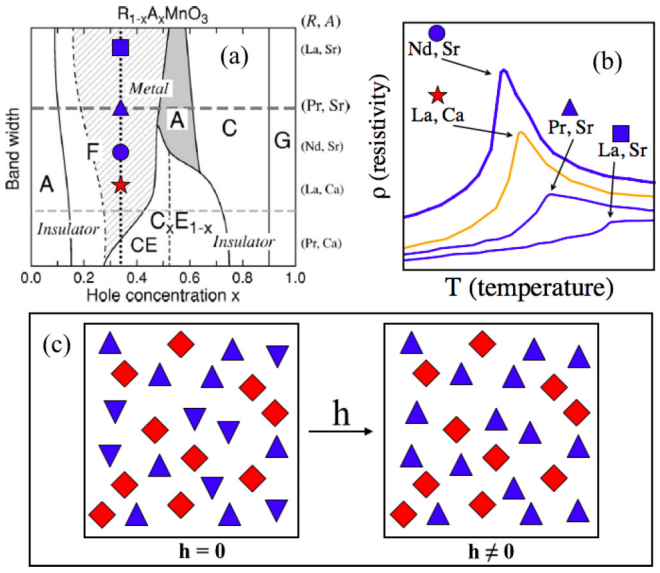

FIG. 1. (a) Schematic low-temperature phase diagram of manganites $R_{1-x}A_xMnO_3$ for different R (rare-earth) and A (alkaline-earth) elements (adopted from Ref. [23]). F, A, and CE-type phases near $x = 1 - n = 0.35$ are of interest in the present study, and they denote ferromagnetic (FM), A-type antiferromagnetic, and CE-type antiferromagnetic phases, respectively. (b) Schematic to illustrate the temperature dependence of the resistivity for different bandwidth manganites at $x = 1 - n \sim 1/3$. The same symbols in (a) and (b) are used to indicate the combination of R and A. (c) Schematic to show the phase coexistence between charge-ordered (red diamonds) and ferromagnetic (blue triangles) nanoclusters without and with a small external magnetic field h above the FM T_c. The direction of a triangle implies the overall spin orientation in each FM nanoclusters (see the text for details).

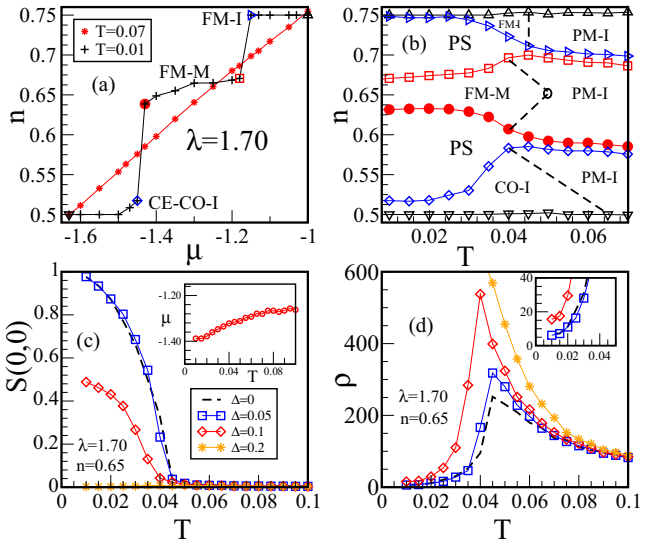

FIG. 2. (a) n dependence on μ for two different temperatures $T = 0.01$ and 0.07. (b) The n-T phase diagram, containing the CO and FM phases. PS, I, and M denote phase separation, insulator, and metal, respectively. The corresponding phase boundaries at $T = 0.01$ are indicated in (a) using the same symbols as in (b). $\Delta = 0$ in (a) and (b). T dependence of (c) the FM structure factor $S(0,0)$ and (d) the resistivity ρ in units of $\hbar a/\pi e^2$ at $n = 0.65$ for different Δ values indicated in (c). The inset in (c) shows the μ vs T, required to set the desired $n = 0.65$. The inset in (d) shows the enlarged plot at low temperatures. $\lambda = 1.7$ for all figures.

Hund's coupling J_H is between t_{2g} spin $\mathbf{S}_i$ and e_g electron spin $\boldsymbol{\sigma}_i$ at site i. Here, we adopt the double-exchange limit, i.e., $J_H \to \infty$, as t (∼0.2–0.5 eV) is estimated to be much smaller than J_H (∼2 eV) [3]. J is the antiferromagnetic superexchange between nearest-neighboring t_{2g} spins. λ represents the electron-phonon coupling between Jahn-Teller phonons $\mathbf{Q}_i$ and e_g electrons in the adiabatic limit. We treat all $\mathbf{S}_i$ and $\mathbf{Q}_i$ as classical variables [34–36], and the stiffness K of Jahn-Teller

TABLE I. Magnetic states observed experimentally at low temperatures [from Fig. 1(a)] for $Pr_{1-x}Ca_xMnO_3$ (PCMO), $La_{1-x}Ca_xMnO_3$ (LCMO), $Nd_{1-x}Sr_xMnO_3$ (NSMO), $Pr_{1-x}Sr_xMnO_3$ (PSMO), and $La_{1-x}Sr_xMnO_3$ (LSMO) at $n = 1 - x = 0.65$ and 0.5. FM-M stands for FM metal. The λ and Δ values used in our calculations to qualitatively reproduce the experimental results and ionic radii of R and A elements [4] are also given.

Experimentally observed magnetic phases				Parameters	
Manganites	Radii (R, A) in Å	$n = 0.65$	$n = 0.5$	λ	Δ
PCMO	1.29, 1.34	CE-type	CE-type	1.75	0.1
LCMO	1.36, 1.34	FM-M	CE-type	1.70	0.05
NSMO	1.27, 1.44	FM-M	CE-type	1.65	0.2
PSMO	1.29, 1.44	FM-M	A-type	1.55	0.2
LSMO	1.36, 1.44	FM-M	FM-M	1.50	0.1

modes and $|\mathbf{S}_i|$ are set to be 1. We also choose a typical value of $J/t = 0.1$ [30]. The effects of disorder are taken into account by the $\sum_i \epsilon_i n_i$ term, where ϵ_i is the quenched binary disorder potential with values $\pm\Delta$. μ is the chemical potential. To analyze the effect of external magnetic field $\mathbf{h} = h\hat{\mathbf{z}}$, wherever necessary, we add a Zeeman coupling term $-\sum_i \mathbf{h} \cdot \mathbf{S}_i$ to the Hamiltonian. We measure λ, Δ, h, and temperature T in units of t.

An exact diagonalization scheme is applied to the mobile e_g electrons in the background of classical spins $\mathbf{S}_i$ and lattice distortions $\mathbf{Q}_i$, and a Monte Carlo method is employed for classical variables. This spin-fermion Monte Carlo method adequately takes spatial fluctuations into account, which is necessary to study the inhomogeneities. To handle large system sizes (up to $N = 24 \times 24$ sites), we employ a Monte Carlo technique based on the traveling cluster approximation [31,33,37]. The randomized classical spins $\mathbf{S}_i$ and lattice distortions $\mathbf{Q}_i$ are annealed starting from a high temperature in an arbitrary quenched disorder configuration. All physical quantities such as magnetization and resistivity are averaged over ten such different disorder configurations in addition to the thermal averages taken during the Monte Carlo simulations.

III. PHASE DIAGRAM ($\lambda = 1.7$ AND $J = 0.1$)

Figures 2(a) and 2(b) show that the ground state is FM metallic in e_g electron density $n = 0.63$–0.67 for $\lambda = 1.7$, and it is separated from the CE-type insulating phase at $n = 0.5$ and the FM insulating phase at $n = 0.75$ [33] by phase-separation

windows at $T = 0.01$. Indeed, n jumps from 0.52 to 0.63 and from 0.67 to 0.75 in the n versus μ curve. However, for high temperatures, n increases monotonically with μ without any discontinuities [see Fig. 2(a) for $T = 0.07$]. Figure 2(b) summarizes the n-T phase diagram in the electron density range $n = 0.5$–0.75, showing different phases.

We focus on $n = 0.65$, which is relevant to the CMR manganites. For this purpose, μ is varied to fix n for different temperatures [inset of Fig. 2(c)]. The temperature dependence of the magnetic structure factor $S(\mathbf{q}) = \frac{1}{N^2}\sum_{ij}\mathbf{S}_i \cdot \mathbf{S}_j e^{i\mathbf{q}\cdot(\mathbf{r}_i-\mathbf{r}_j)}$ at wave vector $\mathbf{q} = (0,0)$ (FM correlations) is shown in Fig. 2(c) for different Δ values. The FM T_c remains the same for $\Delta = 0.05$ as compared to $\Delta = 0$ and decreases for $\Delta = 0.1$. The corresponding resistivity in units of $\hbar a/\pi e^2$ (a is the lattice constant) with temperature obtained by calculating the dc limit of the conductivity using the Kubo-Greenwood formalism [38,39] is shown in Fig. 2(d). The magnitude of the resistivity hump around T_c increases with Δ and its position shifts to the lower temperature. However, the system remains insulating for $\Delta = 0.2$ at all temperatures without any long-range FM order. The intimate correlation between the onset of the ferromagnetism and the resistivity hump indicates that the metallic and the insulating phases compete with each other near T_c.

IV. PHASE COMPETITION ABOVE T_c

To examine the phase competition, a measure of the volume fraction of the CO (or FM) regions is necessary because the structure factors in the momentum space are inefficient to probe the local ordering in the real space. Here we calculate the volume fraction of the $n = 1/2$-type (π,π) CO nanoclusters V(CO) from the real space charge distribution. V(CO) is calculated by counting the fraction of sites for which the local density n_i at site i, satisfying $n_i - 0.5 \geqslant 0.1$, is surrounded by the four nearest-neighbor sites j with $0.5 - n_j \geqslant 0.1$ or vice versa. Similarly, the volume fraction of the FM nanoclusters, V(SO), is obtained by calculating the fraction of sites, say i, for which all $\mathbf{S}_i \cdot \mathbf{S}_j \geqslant 0.5$ with the four nearest-neighboring sites j.

As shown in Figs. 3(a) and 3(c), V(CO) for $\Delta = 0.05$ and 0.1, respectively, increases with decreasing T until T_c and decreases thereafter. The volume fraction of the CO nanoclusters including the next-nearest-neighboring sites, plotted by dotted lines with star symbols in Figs. 3(a) and 3(c), remains very small. Note that V(CO) decreases to zero for $\Delta = 0.05$ but remains finite for $\Delta = 0.1$ at low temperatures. The reminiscence of V(CO) for $\Delta = 0.1$ correlates with the fact that the system is not fully FM even at $T = 0.01$, where $S(0,0) \sim 0.5$ [see Fig. 2(c)]. This shows the fact that the CO nanoclusters coexist with the FM regions for $\Delta = 0.1$ at low temperatures and as a result the resistivity is larger than in the clean systems, as shown in Fig. 2(d).

It is apparently clear from Figs. 3(a) and 3(c) that the resistivity increases with V(CO) until T_c and decreases below it. However, the enhancement of resistivity is steeper than V(CO), which indicates that electrons moving across the system are not only scattered from the CO nanoclusters but also from the FM nanoclusters that may be present in the system. Therefore, the logical next step is to reveal the presence of

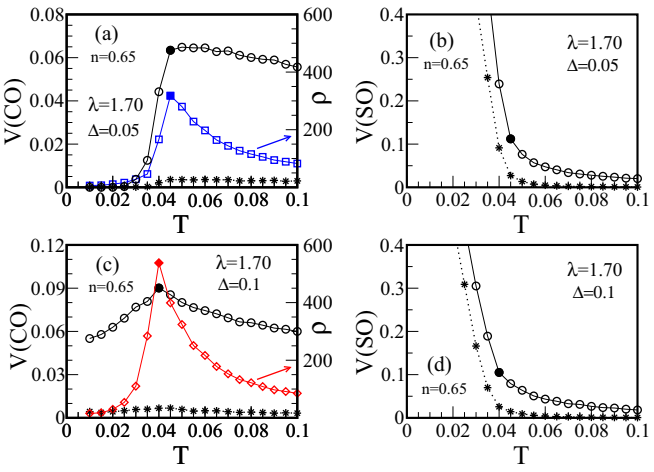

FIG. 3. T dependence of the volume fraction of the CO nanoclusters V(CO) and resistivity ρ (in units of $\hbar a/\pi e^2$) for (a) $\Delta = 0.05$ and (c) $\Delta = 0.1$. The volume fraction of FM nanoclusters V(SO) vs T for (b) $\Delta = 0.05$ and (d) $\Delta = 0.1$. Filled symbols indicate T_c. $n = 0.65$ and $\lambda = 1.7$ for all figures. See the text for dotted lines with star symbols.

FM nanoclusters above T_c. For this purpose, we plot V(SO) in Figs. 3(b) and 3(d). With decreasing T, V(SO) increases up to ~0.1 at T_c and then starts to grow in size. Eventually, the FM nanoclusters merge with each other at low temperatures. This is concluded from the fact that the volume fraction of the FM nanoclusters including the next-nearest-neighbor sites [dotted line with star symbols in Figs. 3(b) and 3(d)] remains very small above T_c, but increases below it for both $\Delta = 0.05$ and 0.1. Typically, the strength of disorder is quantified by the variance of the ionic radii of R and A ions [24,25]. For example, cation mismatch is very small for $La_{1-x}Ca_xMnO_3$ (LCMO). In addition, the ground state of LCMO (at $x \sim 1/3$) is homogeneous [2]. Therefore, we expect that $\Delta = 0.05$ is more appropriate for LCMO (see Table I), and our calculations show FM nanoclusters coexisting with CO nanoclusters above T_c and changes to uniform FM metal at low temperatures.

We now apply a very small external magnetic field h to further confirm the phase coexistence above T_c. For $h = 0.002$, the T_c increases from 0.045 to 0.05 [Figs. 4(a) and 4(b)]. For $T \geqslant 0.05$, V(CO) and V(SO) remain unaffected with h. This indicates that the applied magnetic field does not affect the CO regions, but only aligns spins in different FM nanoclusters without increasing their size, as shown schematically in Fig. 1(c). For $h = 0$, magnetic nanoclusters are randomly oriented. Therefore, in addition to the CO nanoclusters, the up-spin (down-spin) electrons scatter from the down-spin (up-spin) oriented magnetic nanoclusters and the current is carried equally in both spin channels. A small external magnetic field aligns the magnetic nanoclusters, say in the up direction, which decreases the current from the down-spin electrons. This results in an overall enhancement of the resistivity, as shown in Fig. 4(c) using filled symbols, and substantiates the presence of the FM nanoclusters above T_c, in addition to the CO nanoclusters. Such enhancement of resistivity in a magnetic field due to the presence of FM and CO nanoclusters also resembles that with FM-metallic/insulating multilayers in

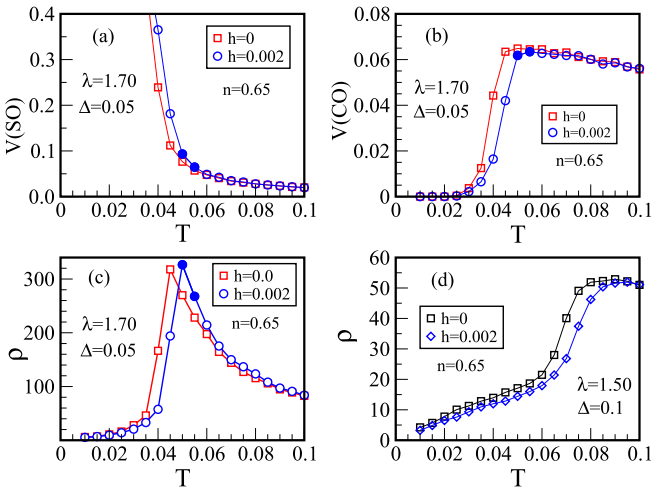

FIG. 4. T dependence of the volume fraction of (a) FM nanoclusters V(SO) and (b) CO nanoclusters V(CO) with and without an external magnetic field h for $\lambda = 1.7$ and $\Delta = 0.05$. Resistivity ρ in units of $\hbar a/\pi e^2$ vs T with and without h for (c) $\lambda = 1.7$ and $\Delta = 0.05$, and (d) $\lambda = 1.5$ and $\Delta = 0.1$. Filled symbols in (a)–(c) highlight that V(SO) and V(CO) remain unaffected, but the resistivity increases for $T = 0.05$ and 0.055 with h.

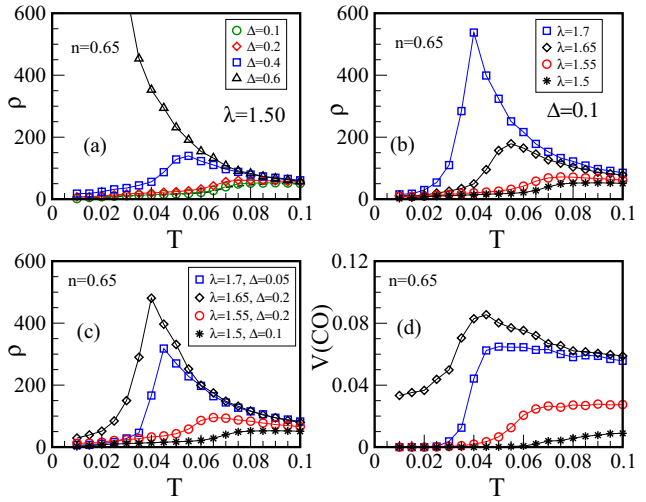

FIG. 6. (a)–(c) T dependence of the resistivity ρ in units of $\hbar a/\pi e^2$ for different parameters (indicated in the figures). In (a), the dashed line is for $\Delta = 0$. (d) Temperature dependence of V(CO) for the same set of parameters used in (c). Legends in (c) and (d) are the same.

which spins in the individual FM layers are randomly oriented [40–42]. In addition, we find in Fig. 4(d) that the resistivity for $\lambda = 1.5$ and $\Delta = 0.1$ does not increase in a small external magnetic field ($h = 0.002$) around T_c ($= 0.075$) because of the absence of CO nanoclusters (discussed below).

Our overall results show that the phase competition between CO and FM nanoclusters above T_c induces the resistivity hump, which is observed in LCMO. However, for large bandwidth manganites, e.g., LSMO (for an abbreviation, see Table I), the resistivity hump diminishes around T_c [see Fig. 1(b)]. To understand this, we show the resistivity and V(CO) for $\lambda = 1.5$, 1.7, and 1.75 in Figs. 5(a) and 5(b), respectively. Recall that λ is measured in units of t, and thus smaller λ corresponds to larger bandwidth or vice versa. For $\lambda = 1.5$ (1.75), the ground state is FM-metallic (CE-type insulating) both at $n = 0.65$ and 0.5, similar to LSMO (PCMO) [see Fig. 1(a)]. A qualitative estimation of λ for different manganites is listed in Table I. For $\lambda = 1.5$, V(CO) is very small and decreases monotonically with decreasing T, resulting in no resistivity hump. This also suggests that the CO nanoclusters above T_c at $n = 0.65$ appear only for

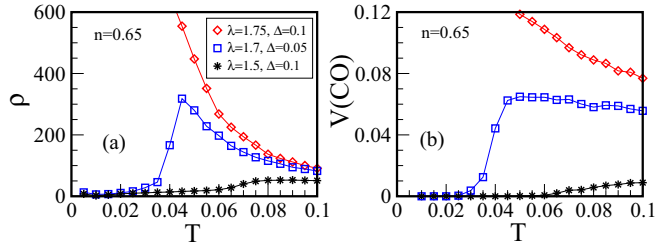

FIG. 5. T dependence of (a) the resistivity ρ in units of $\hbar a/\pi e^2$ and (b) V(CO) for $\lambda = 1.75$, 1.7, and 1.5. Δ values are mentioned in the figure. Legends in (a) and (b) are the same.

specific systems for which the ground state at $n \sim 0.5$ is a CE-type phase. LSMO does not have the CE-type phase at any hole doping unlike LCMO [see Fig. 1(a)], and as a result the resistivity hump vanishes [43]. For $\lambda = 1.75$, for example, small bandwidth manganites such as PCMO V(CO) increase with decreasing T and eventually an insulating state appears at low temperatures. We have considered $\Delta = 0.1$ for LSMO ($\lambda = 1.5$) and PCMO ($\lambda = 1.75$) as the disorder strength is larger than LCMO ($\lambda = 1.7$).

V. COMPARISON WITH EXPERIMENTS

We turn now to explore the impact of disorder. As shown in Fig. 6(a), the resistivity hump appears and the magnitude increases with Δ, even for $\lambda = 1.5$, and its position shifts to lower temperature similar to the case for $\lambda = 1.7$ [Fig. 2(d)]. However, relatively large Δ is required to convert the FM metal to a disorder-assisted insulator for smaller λ. Also, for $\Delta = 0.1$, T_c increases but the magnitude of resistivity hump decreases with decreasing λ (equivalent to increasing the bandwidth) [see Fig. 6(b)]. This is similar to the experiments shown schematically in Fig. 1(b) [43–45] except for NSMO. Although LCMO has a smaller bandwidth than NSMO, the magnitude of the resistivity hump for LCMO is smaller than NSMO. To explain the observed resistivity trend properly, one needs to estimate Δ values correctly, at least qualitatively. Due to the large mismatch between R and A radii, the disorder strength in NSMO is larger than LCMO and thus relatively larger Δ must be set (see Table I). As discussed earlier, Δ for LCMO is minimal, while it increases for LSMO and increases further for NSMO and PSMO. Figure 6(c) shows the resistivity versus temperature for four combinations of λ and Δ values, corresponding to four different manganites (NSMO, LCMO, PSMO, and LSMO) listed in Table I. Resistivity curves in Fig. 6(c) agree qualitatively with the experiments [43–45] shown schematically in Fig. 1(b). This shows that the disorder

also plays an important role in understanding the experimental results systematically. V(CO) plotted in Fig. 6(d) shows a similar trend and clarifies the one-to-one correspondence between the resistivity and the volume fraction of the CO nanoclusters in CMR manganites.

VI. CONCLUSION

In summary, based on the two-band model, we have provided a systematic study to demonstrate the phase competitions between the CO and the FM nanoclusters above T_c in CMR manganites. The resistivity increases due to the enhancement of the volume fraction of the $n = 1/2$-type (π,π) CO and FM nanoclusters, with decreasing T until T_c. The FM nanoclusters start to grow and merge, and they win the competition below T_c, leading to the sharp drop in the resistivity. The CO nanoclusters do not form in large bandwidth manganites, and as a result the resistivity hump vanishes. Our calculations establish a simple yet complete pathway to understand the phase competitions in CMR manganites.

ACKNOWLEDGMENTS

We acknowledge use of the TCMP computer cluster at SINP, and our discussions with P. Majumdar and S. K. Das. Part of the numerical calculations have been done using the computational resource on the HOKUSAI GreatWave supercomputer allocated by RIKEN Advanced Center for Computing and Communication (ACCC).

[1] *Colossal Magnetoresistive Oxides*, edited by Y. Tokura (Gordon and Breach, New York, 2000).
[2] E. Dagotto, *Nanoscale Phase Separation and Colossal Magnetoresistance: The Physics of Manganites and Related Compounds* (Springer, Berlin, 2003).
[3] E. Dagotto, T. Hotta, and A. Moreo, Phys. Rep. **344**, 1 (2001).
[4] Y. Tokura, Rep. Prog. Phys. **69**, 797 (2006).
[5] M. Uehara, S. Mori, C. H. Chen, and S.-W. Cheong, Nature (London) **399**, 560 (1999).
[6] M. Faeth, S. Freisem, A. A. Menovsky, Y. Tomioka, J. Aarts, and J. A. Mydosh, Science **285**, 1540 (1999).
[7] J. M. Zuo and J. Tao, Phys. Rev. B **63**, 060407(R) (2001).
[8] T. Y. Koo, V. Kiryukhin, P. A. Sharma, J. P. Hill, and S. W. Cheong, Phys. Rev. B **64**, 220405(R) (2001).
[9] L. Zhang, C. Israel, A. Biswas, R. L. Greene, and A. de. Lozanne, Science **298**, 805 (2002).
[10] D. D. Sarma, D. Topwal, U. Manju, S. R. Krishnakumar, M. Bertolo, S. La Rosa, G. Cautero, T. Y. Koo, P. A. Sharma, S.-W. Cheong, and A. Fujimori, Phys. Rev. Lett. **93**, 097202 (2004).
[11] S. Chaudhuri, R. C. Budhani, J. He, and Y. Zhu, Phys. Rev. B **76**, 132402 (2007).
[12] J. Tao, D. Niebieskikwiat, M. Varela, W. Luo, M. A. Schofield, Y. Zhu, M. B. Salamon, J. M. Zuo, S. T. Pantelides, and S. J. Pennycook, Phys. Rev. Lett. **103**, 097202 (2009).
[13] Y. Murakami, H. Kasai, J. J. Kim, S. Mamishin, D. Shindo, S. Mori, and A. Tonomura, Nat. Nanotechnol. **5**, 37 (2010).
[14] J. Tao, D. Niebieskikwiat, Q. Jie, M. A. Schofield, L. Wu, Q. Li, and Y. Zhu, Proc. Natl. Acad. Sci. (USA) **108**, 20941 (2011).
[15] M. H. Burkhardt, M. A. Hossain, S. Sarkar, Y.-D. Chuang, A. G. Cruz Gonzalez, A. Doran, A. Scholl, A. T. Young, N. Tahir, Y. J. Choi, S.-W. Cheong, H. A. Duerr, and J. Stoehr, Phys. Rev. Lett. **108**, 237202 (2012).
[16] Y. Horibe, S. Mori, T. Asaka, Y. Matsui, P. A. Sharma, T. Y. Koo, S. Guha, C. H. Chen, and S.-W. Cheong, Europhys. Lett. **100**, 67007 (2012).
[17] N. S. Bingham, P. Lampen, M. H. Phan, T. D. Hoang, H. D. Chinh, C. L. Zhang, S. W. Cheong, and H. Srikanth, Phys. Rev. B **86**, 064420 (2012).
[18] R. Rawat, P. Kushwaha, D. K. Mishra, and V. G. Sathe, Phys. Rev. B **87**, 064412 (2013).
[19] L. Z. Liang, L. Li, H. Wu, and X. H. Zhu, Nanoscale Res. Lett. **9**, 325 (2014).
[20] J. Shao, H. Liu, K. Zhang, Y. Yu, W. Yu, H. Lin, J. Niu, K. Du, Y. Kou, W. Wei, F. Lan, Y. Zhu, W. Wang, J. Xiao, L. Yin, E. W. Plummer, and J. Shen, Proc. Natl. Acad. Sci. (USA) **113**, 9228 (2016).
[21] K. Zhang, L. Li, H. Li, Q. Feng, N. Zhang, L. Cheng, X. Fan, Y. Hou, Q. Lu, Z. Zhang, and C. Zeng, Nano Lett. **17**, 1461 (2017).
[22] C. Martin, A. Maignan, M. Hervieu, and B. Raveau, Phys. Rev. B **60**, 12191 (1999).
[23] R. Kajimoto, H. Yoshizawa, Y. Tomioka, and Y. Tokura, Phys. Rev. B **66**, 180402(R) (2002).
[24] H. Y. Hwang, S-W. Cheong, P. G. Radaelli, M. Marezio, and B. Batlogg, Phys. Rev. Lett. **75**, 914 (1995).
[25] L. M. Rodriguez-Martinez and J. P. Attfield, Phys. Rev. B **63**, 024424 (2000).
[26] A. Moreo, S. Yunoki, and E. Dagotto, Science **283**, 2034 (1999).
[27] E. Dagotto, New. J. Phys. **7**, 67 (2005).
[28] C. Sen, G. Alvarez, and E. Dagotto, Phys. Rev. Lett. **105**, 097203 (2010).
[29] C. Sen, S. Liang, and E. Dagotto, Phys. Rev. B **85**, 174418 (2012).
[30] S. Yunoki, T. Hotta, and E. Dagotto, Phys. Rev. Lett. **84**, 3714 (2000).
[31] S. Kumar, A. P. Kampf, and P. Majumdar, Phys. Rev. Lett. **97**, 176403 (2006).
[32] K. Pradhan, A. Mukherjee, and P. Majumdar, Phys. Rev. Lett. **99**, 147206 (2007).
[33] K. Pradhan, A. Mukherjee, and P. Majumdar, Europhys. Lett. **84**, 37007 (2008).
[34] S. Yunoki, J. Hu, A. L. Malvezzi, A. Moreo, N. Furusaki, and E. Dagotto, Phys. Rev. Lett. **80**, 845 (1998).
[35] E. Dagotto, S. Yunoki, A. L. Malvezzi, A. Moreo, J. Hu, S. Capponi, D. Poilblanc, and N. Furukawa, Phys. Rev. B **58**, 6414 (1998).
[36] S. Yunoki, A. Moreo, and E. Dagotto, Phys. Rev. Lett. **81**, 5612 (1998).
[37] S. Kumar and P. Majumdar, Eur. Phys. J. B **50**, 571 (2006).
[38] G. D. Mahan, *Quantum Many Particle Physics* (Plenum, New York, 1990).
[39] S. Kumar and P. Majumdar, Europhys. Lett. **65**, 75 (2004).

[40] Z. G. Sheng, W. H. Song, Y. P. Sun, J. R. Sun, and B. G. Shen, Appl. Phys. Lett. **87**, 032501 (2005).
[41] T. F. Zhou, G. Li, N. Y. Wang, B. M. Wang, X. G. Li, and Y. Chen, Appl. Phys. Lett. **88**, 232508 (2006).
[42] K. Pradhan and A. P. Kampf, Phys. Rev. B **87**, 155152 (2013).
[43] J. M. D. Coey, M. Viret, L. Ranno, and K. Ounadjela, Phys. Rev. Lett. **75**, 3910 (1995).
[44] E. Saitoh, Y. Okimoto, Y. Tomioka, T. Katsufuji, and Y. Tokura, Phys. Rev. B **60**, 10362 (1999).
[45] N. Furukawa and Y. Motome, J. Phys. Soc. Jpn. **74**, 203 (2005).